

Nonlinear Wigner Solid Transport Over Superfluid Helium Under AC Conditions

Yuriy P. Monarkha^{1,2} and Kimitoshi Kono¹

¹*Low Temperature Physics Laboratory, RIKEN, Hirosawa 2-1, Wako 351-0198, Japan*

²*Institute for Low Temperature Physics and Engineering, 47 Lenin Avenue, 61103 Kharkov, Ukraine*

Nonlinear transport properties of the two-dimensional Wigner solid of surface electrons on superfluid helium are studied for alternating current conditions. For time-averaged quantities like Fourier coefficients, the field-velocity characteristics are shown to be qualitatively different as compared to that found in the DC theory. For a spatially uniform current we found a general solution for the field-velocity relationship which appears to be strongly dependent on the current frequency. If the current frequency is much lower than the ripplon damping parameter, the Bragg-Cherenkov resonances which appear at high enough drift velocities acquire a distinctive saw-tooth shape with long right-side tails independent of small damping. For current frequencies which are close or higher than the ripplon damping coefficient, the interference of ripples excited at different time intervals results in a new oscillatory (in drift velocity) regime of Bragg-Cherenkov scattering.

PACS numbers: 67.90.+z Other topics in quantum fluids and solids; liquid and solid helium; 73.20.-r Electron states at surfaces and interfaces; 73.25.+i Surface conductivity and carrier phenomena.

INTRODUCTION

Electrons trapped on the surface of liquid helium form a clean two-dimensional electron system of which the average Coulomb interaction energy can greatly exceed the average kinetic energy (for a review, see [1, 2]). For typical electron densities realized experimentally ($n_s \lesssim 10^9 \text{ cm}^{-2}$), the Fermi-energy of surface electrons (SEs) is much smaller than temperature. Therefore at a low enough temperature, depending on the surface electron density ($T_c \propto \sqrt{n_s}$), this electron system undergoes a transition to the Wigner solid state. This was first observed by Grimes and Adams [3] from the onset of resonances induced by electron interaction with capillary-waves (ripples) whose wave-vector \mathbf{q} is close to electron reciprocal lattice vectors \mathbf{g} . Since the electron lattice determines a specific set of frequencies $\omega_n = \omega_{g_n}$ [here $n = 1, 2, 3, \dots$, $\omega_q = \sqrt{\alpha/\rho}q^{3/2}$ is the ripplon spectrum, α is the surface tension, and ρ is the mass density of liquid helium], experimental evidence for a triangular electron lattice on a liquid-He surface was given. Electron interaction with such ripples appeared to be very strong, leading to a huge reconstruction of the WS phonon spectrum in the low frequency range [4].

The resonances of Grimes and Adams occur when the frequency of the input signal ω is close to ω_n . Transport properties of the WS of SEs are usually studied under much lower frequencies ($\omega \ll \omega_1$). Nevertheless, even under low frequency conditions the resonant interaction with ripples of frequencies which are close to ω_n appear to be possible as a nonlinear conductivity effect [5]. The physics of this phenomenon can be explained as follows. The pressure at the interface induced by the WS moving with a constant drift velocity \mathbf{v} can be represented as a series of terms proportional to $\exp[i\mathbf{g} \cdot (\mathbf{r} - \mathbf{v}t)]$, where \mathbf{r} is the in-plane coordinate vector. As a function of t , it can be considered as a series of harmonic

perturbations with frequencies $\mathbf{g}\mathbf{v}$, and one can expect a resonance response of the system when $\mathbf{g}\mathbf{v}$ is close to ω_n . It should be noted that the corresponding velocity $v_1 = \omega_1/g_1$ is rather low (typically about $1 - 10 \text{ m/s}$) while the thermal velocity of electrons in the liquid state is usually much higher (about $3 \cdot 10^3 \text{ m/s}$). Therefore the single-electron Cherenkov emission of ripples is a quite usual phenomenon contributing into resistivity of SEs on liquid helium. The important point is that for a moving WS with $\mathbf{g}\mathbf{v} \rightarrow \omega_n$, the response of the system can be considered as a coherent Bragg-Cherenkov (B-C) scattering. This effect was first described by the usual perturbation treatment [6] which leads to symmetrical peaks of the electron collision rate with non-Lorentzian tails.

Besides direct B-C scattering effects limiting the WS velocity [5], there are other interesting nonlinear conductivity (σ) phenomena observed for SE transport over superfluid helium. In the presence of the magnetic field oriented normally to the surface, σ_{xx}^{-1} as a function of the input voltage V has a remarkable N-type anomaly [7]. The decreasing part of $\sigma_{xx}^{-1}(V)$ was attributed to the B-C scattering. When studying WS confined in the channel geometry, periodic conductance oscillations with varying the drift velocity were observed [8]. These oscillations were attributed to anisotropic spatial order with lines of electrons along the channel edges. Complicated nonlinear conductivity of the WS was observed for current frequencies which are close to typical frequencies of plasmon-ripplon coupled modes [9]. Interesting WS velocity jumps caused by the decoupling of electrons from the surface deformation were recently observed for the WS in a channel [10].

Unfortunately, for $q \rightarrow g_1$ the electron-ripplon coupling is strong which leads to a huge increase of the electron effective mass at low frequencies due to surface dimples [4]. Under such conditions the perturbation treatment is doubtful and coupled WS phonon-ripplon modes

are usually treated in a self-consistent way [11, 12]. In this treatment the most of the interaction Hamiltonian of the WS with ripples of $q \rightarrow g_1$ is included in the description of the coupled modes. Therefore, a simple classical model of coherent B-C scattering of capillary waves for the WS moving with a constant velocity [13] seems to be more appropriate than a perturbation treatment. This model was introduced in order to analyze a complicated nonlinear magnetoconductivity observed previously [7]. An extension of this model applied to liquid ^3He allows to explain the nonlinear field-velocity characteristics of the WS under strong ripplon damping conditions [14, 15].

Application of the models of coherent B-C scattering to the nonlinear WS transport on liquid ^4He is difficult for several reasons. First, experimental geometries usually imply that the driving electric field and electron current density are not spatially uniform. Secondly, measurements are done under AC conditions when the electron velocity and driving electric field are periodic functions of time with the period $2\pi/\omega$ which is much longer than the typical ripplon oscillation period $2\pi/\omega_1$. Moreover, the damping of ripples γ_q in superfluid ^4He is anomalously small [16], which means that B-C peaks of the classical model are extremely narrow and some other effects not included in the model can significantly affect its main results.

In this work we study the surface-displacement profile and field-velocity relationship for spatially uniform alternating motion of the WS over superfluid ^3He and ^4He under small ripplon damping conditions: $\gamma_{g_1} \ll \omega_1$. For arbitrary frequency of the current ω , the exact expression for the field-velocity relationship can be found. This solution appears to be strongly dependent on the ratio ω/γ_g . Therefore, we separate two frequency regions: $\omega \ll \gamma_g$ and $\omega \gtrsim \gamma_g$. In both regions, the nonlinear field-velocity characteristics obtained here for time averaged quantities differ significantly from those obtained in the DC model. In the high frequency region $\gamma_g \lesssim \omega \ll \omega_g$, we expect the appearance of a new B-C scattering regime of the WS transport caused by interference of ripples excited at different time intervals. This frequency region is usually realized in experiments on nonlinear WS transport over superfluid ^4He , and, therefore, we expect that our new results will help to understand the nonlinear electronic response observed.

DIMPLE PROFILE EVOLUTION INDUCED BY THE DRIFT VELOCITY

The analysis of the classical B-C scattering given in Ref. [13] was restricted to a simplified one-dimensional DC model. The damping effects were considered in a phenomenological way. Here we consider more realistic 2D model of alternating motion of the WS with a particular ripplon damping defined for both ^3He and ^4He .

We investigate shape variations induced by the WS velocity and ripplon damping which are very important for understanding the nonlinear WS transport.

We assume spatially uniform motion of the WS, which means that all electron lattice sites have the same displacement vector $\mathbf{s}(t)$ in external fields. In this case the electron pressure at the interface induced by the WS moving with an arbitrary velocity can be presented in the following form:

$$P^{(el)}(\mathbf{r}, t) = n_s \sum_{\mathbf{g}} \tilde{V}_g \exp[i\mathbf{g} \cdot (\mathbf{r} - \mathbf{s}(t))], \quad (1)$$

where $\tilde{V}_g = V_q \exp(-q^2 \langle u_f^2 \rangle / 4)$, the electron-riplon coupling V_q depends on the holding electric field E_{\perp} directed normally to the surface and on the wavenumber q [2], and $\langle u_f^2 \rangle$ - is the mean-square displacement of electrons from lattice sites due to fast coupled phonon-riplon modes whose frequencies are limited by $\omega_f \gg \omega_1$. Actually, ω_f is the frequency of electron oscillations in the potential of a steady dimple. A simple self-consistent treatment [12] gives

$$\langle u_f^2 \rangle \simeq \frac{\langle u_0^2 \rangle + u_T^2 \ln(T/\hbar\omega_V)}{1 - g_1^2 u_T^2 / 4}, \quad (2)$$

where $\langle u_0^2 \rangle \simeq 1.248\hbar/(2m_e c_t \sqrt{\pi n_s})$ is the mean-square displacement due to zero point vibrations,

$$u_T^2 = \frac{T}{2\pi m_e n_s c_t^2}, \quad \omega_V = \sqrt{\frac{3n_s}{\alpha m_e}} V_{g_1}, \quad (3)$$

m_e is the free electron mass, and c_t^2 is the transverse sound velocity of the electron solid.

Considering ripples as an ensemble of surface oscillators with a certain damping parameter γ_q surface displacements $\xi(\mathbf{r})$ induced by pressure perturbations of Eq. (1) can be found in a quite general form:

$$\xi_{\mathbf{g}}(t) = -\frac{n_s g \tilde{V}_g}{\rho \cdot \hat{\omega}_g} \int_{-\infty}^t \sin[\hat{\omega}_g(t-t')] \times \exp[-i\mathbf{g} \cdot \mathbf{s}(t') + \gamma_g(t'-t)] dt', \quad (4)$$

where $\hat{\omega}_g = \sqrt{\omega_g^2 - \gamma_g^2}$. Here we extend the treatment given in Ref. [2] into the range of a finite but small ripplon damping. For AC conditions $\mathbf{s}(t) = \mathbf{s}_0 \sin(\omega t)$. Introducing the new variable $\tau = t' - t$ and assuming $\omega\tau \ll 1$ we represent $\mathbf{s}(t') \approx \mathbf{s}(t) + \mathbf{v}(t)\tau$. In this approximation surface displacements can be found as

$$\xi_{\mathbf{g}}(t) = -\frac{n_s g \tilde{V}_g}{\rho [\omega_g^2 - (\mathbf{g}\mathbf{v})^2 - 2i\gamma_g \mathbf{g}\mathbf{v}]} e^{-i\mathbf{g} \cdot \mathbf{s}(t)}, \quad (5)$$

where $\mathbf{v} = \mathbf{s}_0 \omega \cos(\omega t)$ is the WS velocity. This equation represents dimple sublattice moving in-phase with the WS. In the limit $\mathbf{g}\mathbf{v} \rightarrow 0$, Eq. (5) surely gives the well

known shape of steady dimples which is independent of damping. If $\mathbf{g}\mathbf{v} \sim \omega_g$, the shape of dimples is affected by the WS velocity and damping. Thus, under the condition $\omega\tau \ll 1$, which according to Eq. (4) requires $\omega \ll \gamma_g$, the dimple shape changes with time continuously in such a way that it is always adjusted to a given velocity $\mathbf{v}(t)$. In other words, for any fixed value of $\mathbf{v}(t)$ the dimple shape is the same as that defined by the DC theory with the corresponding WS velocity.

For liquid ^3He , the weak ripplon-damping regime can be realized only for superfluid phase at $T < 0.3$ mK. In this case, γ_g is determined by ballistic bulk quasiparticle scattering from an uneven interface [15]:

$$\gamma_q = \frac{\hbar(k_F)^4}{8\pi^2\rho} 2f(\Delta/T)q, \quad (6)$$

where k_F is the Fermi momentum of quasiparticles in liquid ^3He , Δ is the excitation gap, and $f(x) = (e^x + 1)^{-1}$. The ripplon damping of superfluid ^3He decreases with cooling at an exponential rate. Still, in experiments on WS it can be just reasonably small ($\gamma_g/\omega_g \sim 0.1$ or 0.01).

In contrast, the ripplon damping in superfluid ^4He is anomalously small. In the ballistic regime it is given by [16]

$$\gamma_q = \frac{\pi^2 \hbar}{60 \rho} \left(\frac{T}{\hbar v_{4\text{He}}} \right)^4 q, \quad (7)$$

where $v_{4\text{He}}$ is the first sound velocity. For $n_s = 10^9 \text{ cm}^{-2}$ and $T = 0.5$ K, a simple estimate gives $\gamma_{g_1}/\omega_{g_1} \sim 10^{-4}$. Thus, for WS transport on superfluid ^4He the damping coefficient of ripples is extremely small. It is remarkable that this damping coefficient has the same dependence on the wave-vector q as that found for the ballistic regime of liquid ^3He [Eq. (6)].

In the reference frame moving along with the WS, the dimple profile given by Eq. (5) can be evaluated as

$$\xi(\mathbf{r}) = - \sum_{\mathbf{g}} \frac{n_s g \tilde{V}_g}{\rho |D_{\mathbf{g}}(\mathbf{v})|^2} [(\omega_g^2 - (\mathbf{g}\mathbf{v})^2) \cos(\mathbf{g}\mathbf{r}) - 2\mathbf{g}\mathbf{v}\gamma_g \sin(\mathbf{g}\mathbf{r})], \quad (8)$$

where $D_{\mathbf{g}}(\mathbf{v}) = \omega_g^2 - (\mathbf{g}\mathbf{v})^2 - i2\mathbf{g}\mathbf{v}\gamma_g$. At low temperatures, especially for superfluid ^3He , the summation over a large number of \mathbf{g} is necessary to ensure the convergence of the result. Consider $\mathbf{r} = (x, 0)$ and assume that the driving force $-e\mathbf{E}$ is directed along to the x -axis. Then, according to Eq. (8), in the absence of damping, dimples have a symmetrical shape with regard to electron lattice sites. A finite damping introduces asymmetry in the dimple shape due to the terms proportional to $\sin(g_x x)$.

Shape variations of surface dimples induced by a finite WS velocity are very sensitive to orientation of the vector \mathbf{v} with regard to symmetry axes of the WS. We shall consider the following two typical directions. The

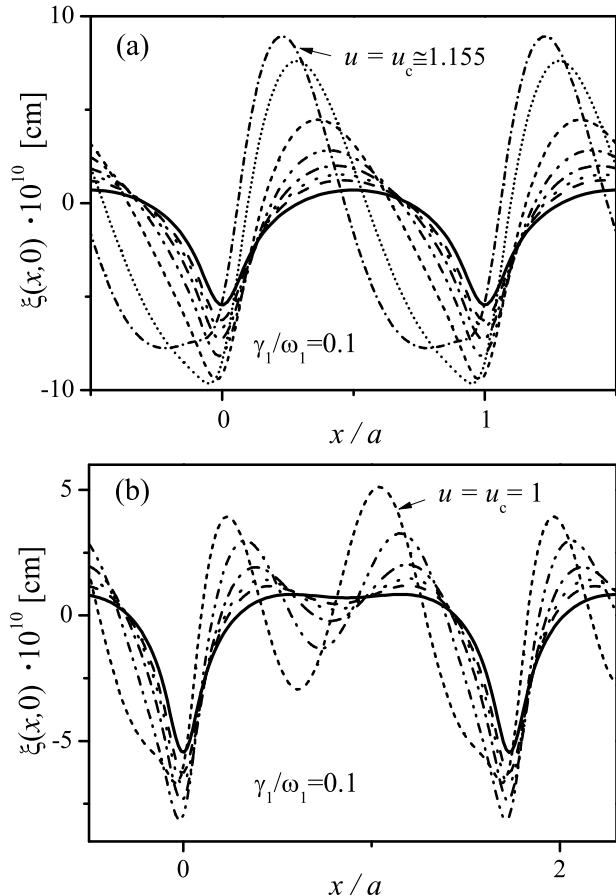


FIG. 1: Variations of the dimple sublattice profile $\xi(x, 0)$ induced by the WS velocity for two typical velocity orientations: NN-direction (a), and SN-direction (b). Steady dimples are shown by the solid line. The dimensionless velocity increases from $u = 0.6$ to higher values by steps equal 0.1. Calculations are performed for superfluid ^3He , $n_s = 10^8 \text{ cm}^{-2}$, $E_{\perp} = 189 \text{ V/cm}$, and $T = 0.277 \text{ mK}$ ($\gamma_1/\omega_1 = 0.1$).

direction of the vector \mathbf{v} which is parallel to the line connecting two nearest neighbors of the electron lattice will be called NN-direction. The direction of \mathbf{v} which is parallel to the line connecting second neighbors will be called SN-direction. If the ripplon damping coefficient γ_1 is not too small (about $0.1 \cdot \omega_1$), the asymmetrical variations of the dimple shape start already at substantial shifts from the B-C resonance as shown in Fig. 1 (a and b) for two typical directions of the velocity vector. Here the dimple shape of a motionless WS is shown by the solid line. The first shape-line (dashed) of moving dimples is calculated for dimensionless velocity $u = v/v_1 = 0.6$ (here $v_1 = \omega_{g_1}/g_1$). For each next curve shown in this figure, the parameter u is increased by steps equal 0.1 except for the curve calculated at $u = 2/\sqrt{\pi}$. The last curve is

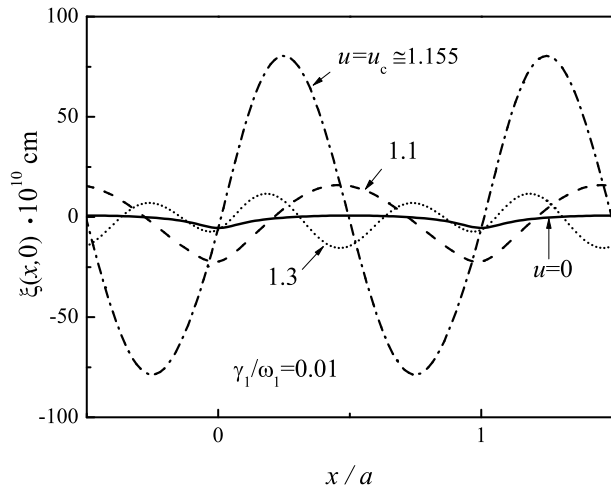


FIG. 2: Variations of the dimple sublattice profile $\xi(x,0)$ induced by the WS velocity near the first B-C resonance for very small ripplon damping $\gamma_1/\omega_1 = 0.01$. The drift velocity is oriented along the NN-direction. Calculations are performed for superfluid ${}^3\text{He}$, $n_s = 10^8 \text{ cm}^{-2}$, $E_\perp = 189 \text{ V/cm}$, and $T = 0.2 \text{ mK}$.

calculated for the critical velocity u_c of the first B-C resonance, which equals 1 for the SN-direction (Fig. 1b), and $2/\sqrt{\pi}$ for the NN-direction (Fig. 1a). For the symmetrical dimple shape, the average force acting on electrons is obviously zero. The strong shape asymmetry appears in order to transfer the kinetic friction acting on the dimple sublattice by the environment to the electron crystal.

For significantly smaller damping coefficient $\gamma_1 = 0.01 \cdot \omega_1$, which is expected for superfluid ${}^3\text{He}$ at $T = 0.2 \text{ mK}$, substantial shape changes appear only if the WS velocity approaches the first B-C resonance or exceeds it. Dimple shape variations which occur near the vicinity of the first resonance are shown in Fig. 2. The important point is that the velocity-induced displacements found for $u = u_c = 2/\sqrt{\pi}$ are much larger (about 15 times) than surface displacements in the initial surface dimple. This means that dynamic decoupling of the WS from surface dimples which shall be discussed below for a fixed field condition is accompanied by creation of huge displacement waves moving in the same direction.

At $u < u_c$, in spite of huge changes of the dimple profile the average position of an electron remains the same being fixed to the potential minimum formed by the dimple potential and the driving electric field. For experimental conditions with a given current, we may consider the evolution of surface dimple profile even at $u > u_c$. For example, at $u = 1.3$ surface displacements induced by the WS velocity are already substantially reduced, still their amplitude is larger than the initial dimple depth.

It is instructive to consider dimple shape variations in-

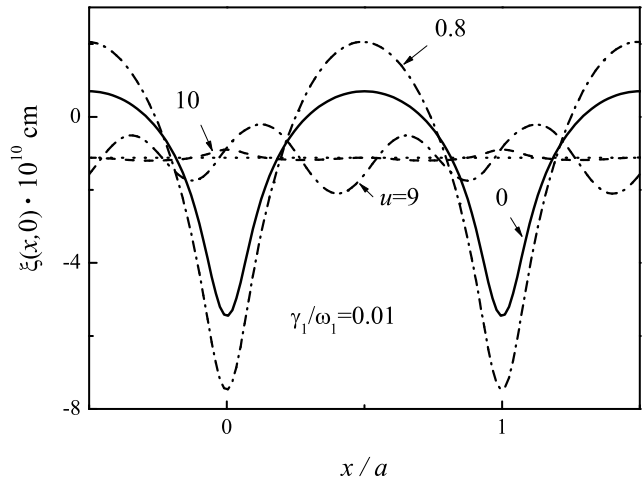


FIG. 3: Variations of the dimple sublattice profile $\xi(x,0)$ induced by the WS velocity away from the first B-C resonance condition for $\gamma_1/\omega_1 = 0.01$. The drift velocity is along the SN-direction. Other conditions are the same as in Fig. 2.

duced by WS velocity which is away from the first B-C resonance condition. The corresponding calculations are shown in Fig. 3. As expected, at $u = 0.8 < u_c$ the WS velocity just increases the dimple depth. Significantly faster velocities $u \sim 10$ cause the opposite effect: the surface displacements are substantially reduced. For $u = 9$ we accidentally reached one of higher B-C resonances, causing strong asymmetry in the dimple shape. A small detuning up to $u = 10$ makes the shape nearly symmetrical which means that the force transferred to the WS by dimples is close to zero. It is instructive that in the limit $u \rightarrow \infty$ surface displacements still remains as shown in Fig. 3 by the straight dotted line, but instead of individual dimples we have a row of interface valleys oriented in the direction of motion.

Shape variations induced by B-C resonances lead to strong changes in the associated mass of an electron dimple M_d which is given by

$$M_d(\mathbf{v}) = \frac{n_s}{\rho} \sum_{\mathbf{g}} \frac{g_x^2 g \tilde{V}_g^2}{(\omega_g^2 - (\mathbf{g}\mathbf{v})^2)^2 + (2\gamma\mathbf{g}\mathbf{v})^2}, \quad (9)$$

where \mathbf{v} is directed along the x -axis. For a finite thickness of the liquid helium d , each term in the sum should be multiplied by $\coth(gd)$. Obviously, the B-C resonances increase the associated mass of a surface dimple. In the limiting case $\mathbf{g}\mathbf{v} \rightarrow \infty$, the associated mass $M_d(\mathbf{v})$ disappears because the dimple lattice is rearranged in a row of valleys (terms with $\mathbf{g}\mathbf{v} = 0$ do not contribute in M_d because of the proportionality factor g_x^2).

FIELD-VELOCITY CHARACTERISTICS

The asymmetry of the dimple shape with regard to the average electron position in a lattice site causes a force $\mathbf{F}^{(D)}$ acting on the electron solid. In equilibrium this force is balanced by an external driving field. By definition, $\mathbf{F}^{(D)}$ is the sum of forces acting on each electron $-\sum_e \partial V_{\text{int}}/\partial \mathbf{r}_e$ averaged over electron distribution within the dimple [here $V_{\text{int}}(\mathbf{r})$ is the electron-rippion interaction Hamiltonian whose Fourier transform V_q was used in Eq. (1)]. Electron distribution caused by long wave-length fluctuations with $\omega < \omega_1$ occurs together with surface dimples and therefore it should be excluded from the averaging. Then, the average of the electron density operator $n_{-\mathbf{q}} = \sum_e \exp(i\mathbf{q}\mathbf{r}_e)$ can be found as

$$\langle n_{-\mathbf{q}} \rangle_f = N_e \exp[-q^2 \langle u_f^2 \rangle / 4 + i\mathbf{q} \cdot \mathbf{s}(t)] \delta_{\mathbf{q}, \mathbf{g}}. \quad (10)$$

Using this equation and Eq. (4) in the general expression $-\langle \sum_e \partial V_{\text{int}}/\partial \mathbf{r}_e \rangle_f$, the force acting on the WS can be written as

$$F^{(D)}(t) = -N_e \sum_{\mathbf{g}} \mathbf{g} \frac{n_s g \tilde{V}_g^2}{\rho \hat{\omega}_g} \int_0^\infty \sin(\hat{\omega}_g \tau) e^{-\gamma_g \tau} \times \\ \times \sin\{\mathbf{g}[\mathbf{s}(t) - \mathbf{s}(t - \tau)]\} d\tau. \quad (11)$$

For any spatially uniform displacement $\mathbf{s}(t)$ given, this equation defines the in-plane force induced by the dimple sublattice.

If the time scale of the WS displacement vector $\mathbf{s}(t)$ is much longer than $\tau \sim 1/\gamma_g$, then $\mathbf{g}[\mathbf{s}(t) - \mathbf{s}(t - \tau)]$ can be approximated by $\mathbf{g}\mathbf{v}(t)\tau$. In this limit $\mathbf{F}^{(D)}$ has the same form as that given by the DC treatment with the constant velocity replaced by $\mathbf{v}(t)$. In equilibrium, $F_{(x)}^{(D)}$ as well as the kinetic friction of the electron lattice $F_{(x)}^{(\text{fric})} = -N_e \nu_e v$ caused by electron scattering of other kinds are balanced by the external force $N_e e E$ (here we assume that magnetic field is zero). The solution of the balance equation can be represented as a field-velocity characteristic $E(\mathbf{v})$:

$$E(\mathbf{v}) = \frac{n_s}{e\rho} v \sum_{\mathbf{g}} \frac{g_x^2 g \tilde{V}_g^2 2\gamma_g}{(\omega_g^2 - g_x^2 v^2)^2 + 4\gamma_g^2 g_x^2 v^2} + \frac{m_e \nu_e}{e} v. \quad (12)$$

Using this equation, $E(\mathbf{v})$ can be calculated numerically for any given damping coefficient and the collision frequency ν_e caused by electron scattering with thermal ripples, vapor atoms, or even walls if WS is formed in a channel geometry.

For the DC case, Eq. (12) is a two-dimensional extension of the classical one-dimensional model of B-C scattering reported previously [13] with the real ripplon damping parameter and with more accurate electron-rippion coupling. The driving field found from the balance equation has sharp maxima in the vicinity of B-C

resonance conditions $g_x^2 v^2 \rightarrow \omega_g^2$. If the driving field is given and the WS velocity is adjusted to the field, then regions with $dE/dv < 0$ are unstable. This means that for driving fields exceeding the major maximum of $E(\mathbf{v})$ the balance of forces is not possible and the WS decouples from surface dimples. According to Fig. 2, decoupling of the WS is accompanied by creation of huge surface waves moving with the group velocity u_c .

In experiments on WS transport, usually it is the current which is given, while the driving field is adjusted to the current by electron redistribution which screens the external potential variations. This is supported by the fact that regions with $dE/dv < 0$ are experimentally observed [8, 14]. Therefore, field-velocity characteristics of electrons moving ultra-fast with $u > u_c$ are very important for understanding the nonlinear WS transport on superfluid helium.

For liquid ^4He with $\gamma_g/\omega_g \sim 10^{-4}$, Eq. (12) applied to the DC case would give just a set of extremely sharp peaks. At the same time, beyond these peaks $E(\mathbf{v})$ is close to zero. For liquid ^3He , the parameter γ_g/ω_g can be much larger than it is for liquid ^4He (even larger than unity) and B-C peaks of $E(\mathbf{v})$ can substantially overlap. It is worth noting that $E(\mathbf{v})$ depends strongly on the velocity vector orientation with regard to the 2D electron lattice. For example, in the NN-direction of motion there is only one major peak with $|\mathbf{g}| = g_1$ at $u = 2/\sqrt{\pi}$, while for the SN-direction there are two equivalent peaks with $|\mathbf{g}| = g_1$ at $u = 1$ and $u = 2$.

In contrast to models of B-C scattering discussed previously, the real experimental situation has one unavoidable complication: DC measurements are practically impossible and by now all data are obtained under AC conditions. This means that WS velocity and the driving electric field are periodic functions of time with the period $2\pi/\omega$. The frequency of experimental signal is usually varies from 10^4 s^{-1} to about $6 \cdot 10^5 \text{ s}^{-1}$ which is much lower than the typical ripplon frequency ω_1 . Therefore, it is conventionally expected that the DC model of WS transport should give qualitatively correct description of data obtained in such experiments. We shall see that this is not true for two major reasons.

First, we note that the condition $\omega \ll \omega_1$ is not sufficient for adiabatic adjustment of surface displacements to WS velocity variations. For example at the B-C resonance condition ($u = u_c$) we have a huge wave which follows the WS and for a change to much smaller displacements a shape variation (without changing the amplitude) is not sufficient. At the B-C resonance the capillary wave accumulates great energy which should be transferred to the environment in order to make the transition from the surface displacements calculated for $u = u_c \simeq 1.155$ (see Fig.) to the surface displacements calculated for $u = 1.3$ or even for $u = 1.1$. This means that an adiabatic AC extension of the DC model requires an additional restriction: the frequency of the current

should be much lower than the corresponding ripplon damping ($\omega \ll \gamma_1$). This is actually the condition which allowed us to transform Eq. (11) into Eq. (12). For WS transport over superfluid ^3He this condition is satisfied even at $\gamma_g/\omega_g \sim 10^{-2}$. Regarding liquid ^4He , the condition $\omega \ll \gamma_1$ requires to use an AC frequency which is much lower than 10^4 s^{-1} .

Secondly, even if the above noted condition is fulfilled, Eq. (12) cannot be used directly for plotting field velocity characteristics. Under AC conditions, it is important which quantities are actually measured and presented in the field-velocity characteristics. If time averaged quantities are considered, in the nonlinear regime the outcome can be qualitatively different for different kinds of averaging. For example, even for harmonic velocity $u_0 \cos \omega t$, the mean-square time averaging of the driving field $\sqrt{\langle E^2 \rangle}$ and averaging of the absolute value $\langle |E| \rangle$ give qualitatively different results for the function $E(u_0 \cos \omega t)$ defined by Eq. (12). This could be easily proven by considering the right-side tail of the B-C resonance in the limiting case $\gamma_g \rightarrow 0$. For averaging $|E|$, in this limit a part of the corresponding integrand can be rearranged as the δ -function [see Eq. (12)], and the final result will not depend on γ_g . In contrast, the integrand of the quantity $\langle E^2 \rangle$ is squared, and, therefore, the resonance tail of $\sqrt{\langle E^2 \rangle}$ increases with reducing γ_g .

As a measure of the alternating field one can choose the main term of the Fourier series representing $E(t)$:

$$E_\omega = \frac{\omega}{\pi} \int_{-\pi/\omega}^{\pi/\omega} E(t) \cos(\omega t) dt. \quad (13)$$

It is also a kind of time averaging, and similar to $\langle |E| \rangle$ it has a finite resonance tail in the limiting case $\gamma_g \rightarrow 0$. In the following we shall consider only quantities E_ω and $\langle |E| \rangle$ which will be used for presenting the field-velocity relationship.

Assume that the conditions of given current is realized and $u(t) = u_0 \cos \omega t$. Using the adiabatic treatment discussed above, we insert $v(t) = v_1 u(t)$ into Eq. (12) and evaluate the time integral of Eq. (13). It is convenient to introduce two integer variables m and n to describe the reciprocal lattice vectors $\mathbf{g}_{m,n} = m\mathbf{g}^{(1)} + n\mathbf{g}^{(2)}$ (here $\mathbf{g}^{(1)}$ and $\mathbf{g}^{(2)}$ are primitive vectors of this lattice). Then, after some algebra, the Fourier transform E_ω can be represented as a function of the velocity amplitude

$$E_\omega(u_0) = v_1 \frac{n_s \rho^{1/2}}{e \alpha^{3/2} g_1} \sum_{m,n} \frac{p_{m,n} \tilde{V}_{g_{m,n}}^2}{g_{m,n}^{1/2}} Q(p_{m,n} u_0, \beta_{m,n}) + \frac{m_e \nu_e}{e} v_1 u_0. \quad (14)$$

Here we use the following dimensionless notations

$$p_{m,n} = \frac{\sqrt{(\mathbf{g}_{m,n})_x^2}}{g_1} \left(\frac{g_1^3}{g_{m,n}^3} \right)^{1/2}, \quad \beta_{m,n} = 2 \frac{\gamma_{g_{m,n}}}{\omega_{g_{m,n}}}, \quad (15)$$

$$Q(w, \beta) = \frac{4w\beta}{\pi} \int_0^\infty \frac{dy}{\left[(1+y^2-w^2)^2 + w^2\beta^2(1+y^2) \right]}. \quad (16)$$

The integral $Q(w, \beta)$ can be evaluated in an analytical form:

$$Q(w, \beta) = \frac{2\beta}{wG} \text{Re} \left[\frac{1}{\sqrt{w^2-1-w^2\beta^2/2-iw^2G}} \right], \quad (17)$$

where $G(\beta) = \beta\sqrt{1-\beta^2/4}$. Remarkably, in the limit $\gamma_g \rightarrow 0$ ($\beta \rightarrow 0$) for $w > 1$ there is a finite asymptote

$$Q(w, \beta) \rightarrow \frac{2\theta(w-1)}{w\sqrt{w^2-1}}, \quad (18)$$

where $\theta(x)$ is the unit step-function.

For $\langle |E| \rangle$ as a function of the dimensionless velocity amplitude u_0 , an equation similar to Eq. (14) is found. The only difference which appears for such averaging is that instead of $Q(w, \beta)$ we should use another function $I(w, \beta)$ defined by

$$I(w, \beta) = \frac{2\beta}{\pi G} \text{Re} \left[\frac{\arctan \left[\frac{iw}{\sqrt{w^2-1+\beta^2/2+iG}} \right]}{\sqrt{w^2-1+\beta^2/2+iG}} \right], \quad (19)$$

As expected in the limiting case $\gamma_g \rightarrow 0$ ($\beta \rightarrow 0$), it also has a finite asymptote

$$I(w, \beta) \rightarrow \frac{\theta(w-1)}{\sqrt{w^2-1}}, \quad (20)$$

which means that the right-side tails of B-C resonances are independent of small damping.

Already from the analysis of the integrals $Q(w, \beta)$ and $I(w, \beta)$ given above one can conclude that B-C resonance tails of the AC treatment differ (even qualitatively) from that found for the DC models. The left-side tail becomes even steeper for both $E_\omega(u_0)$ and $\langle |E| \rangle$, while the right-side tails extend far beyond the resonance and are independent of ripplon damping in the limit $\gamma_g \rightarrow 0$. This behavior is illustrated in Fig. 4 where $E_\omega(u_0)$ is plotted for two typical directions of the WS velocity [NN-direction (solid line), and SN-direction (dashed line)] assuming $\gamma_g \rightarrow 0$. The other parameters are taken for the liquid ^4He case. Thus, instead of δ -peaks of the classical B-C scattering model here we have saw-tooth shaped peaks with long right-side tails. As noted above, field-velocity characteristics depend strongly on the direction of the WS velocity. It is interesting that for the SN-direction there are two major B-C peaks and the second one (at $u_0 \rightarrow 2$) becomes even more prominent than the first one because in the AC cause at $u_0 > 2$ the velocity sweeps through the both resonances. Of course, considering the limiting case $\gamma_g/\omega_1 \rightarrow 0$ we should keep in mind that ω should be much smaller than γ_g . Therefore, real

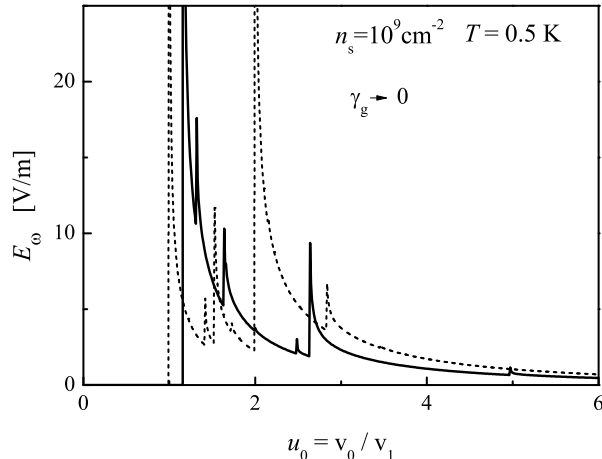


FIG. 4: The first Fourier coefficient of the driving field E_ω vs the drift velocity amplitude for two typical orientations of the velocity: NN-direction (solid line) and SN-direction (dashed line). Calculations were performed for superfluid ^4He , $n_s = 10^9 \text{ cm}^{-2}$, $T = 0.5 \text{ K}$, assuming the ripplon damping is set to zero.

riplon damping should be taken into account for consistent analysis of field-velocity relationships induced by B-C scattering.

For nonlinear WS transport over superfluid ^4He , the ripplon damping parameter is extremely small and the condition $\gamma_g < \omega \ll \omega_g$ is realized in most of known experiments. This case requires a special treatment because large surface displacements excited at a first instance of $u(t) = u_c$ cannot be relaxed back within the period of current oscillations. Therefore a new steady regime will be developed for each AC frequency, which can be far away from the solutions found above for the condition $\omega \ll \gamma_g$.

We have to return back to the exact solution of Eq. (11). In this equation now we insert $s_x(t) = (v_0/\omega) \sin(\omega t)$ and then perform the time averaging defined by Eq. (13). Here we disregard the unimportant correction induced by ν_e . Then quite generally, $E_\omega(v_0)$ can be found as

$$E_\omega(v_0) = \sum_{\mathbf{g}} \frac{g_x n_s g \tilde{V}_g^2}{e \rho \hat{\omega}_g} 2 \int_0^\infty \sin(\hat{\omega}_g \tau) e^{-\gamma_g \tau} \cos\left(\frac{\omega \tau}{2}\right) \times J_1 \left[2g_x \frac{v_0}{\omega} \sin\left(\frac{\omega \tau}{2}\right) \right] d\tau, \quad (21)$$

where $J_1(z)$ is the Bessel function of the first kind. For E_ω as a function of the dimensionless velocity amplitude u_0 , an equation similar to Eq. (14) can be found. In the general case, the integral $Q(w, \beta)$ of Eq. (14) should be

replaced by $Q(w, \beta, \omega')$ defined as

$$Q(w, \beta, \omega') = 4 \int_0^\infty \sin(2y) e^{-\beta y} \cos(\omega' y) \times J_1 \left[2 \frac{w}{\omega'} \sin(\omega' y) \right] dy, \quad (22)$$

where $\omega' = \omega/\hat{\omega}_g$. The dimensionless function $Q(w, \beta, \omega')$ describes the shape of a single B-C resonance of $E_\omega(u_0)$ for arbitrary current frequency and ripplon damping (here $w \propto u_0$ and $\beta \propto \gamma_g$). It is easy to see that in the limiting case $\omega' \rightarrow 0$ and $\beta \rightarrow 0$ analyzed above, Eq. (22) provides the correct asymptote shown in Eq. (18). For conditions $\gamma_g < \omega \ll \omega_g$, and $g_x v_0 > 1$, the argument of the Bessel function entering the integrand of Eq. (21) attains huge numbers because $\sin(\omega\tau/2) \sim 1$. This can lead to remarkable field-velocity relationships with side-oscillations which we shall discuss in the following.

RESULTS AND DISCUSSIONS

Consider briefly the velocity-field relationship $E_\omega(u)$ for WS transport over superfluid ^3He at $T = 0.25 \text{ mK}$. At such a temperature the damping coefficient $\gamma_{g1} \simeq 1.54 \cdot 10^6 \text{ s}^{-1}$ is much lower than the B-C resonance frequency ω_1 and is still much higher than the typical current frequency ω used in experiments. The later condition makes the adiabatic AC extension of the B-C scattering model introduced here applicable. The results of numerical evaluations of Eq. (14) are shown in Fig. 5. The velocity-field characteristic given by the DC classical model is shown by the dotted line. It consists of series of B-C peaks with nearly symmetric tails. For the first Fourier coefficient as a function of the drift velocity amplitude, the AC theory gives lower peaks which are asymmetric with regard to the maximum positions. It is important that time averaging used in evaluation of $E_\omega(u_0)$ do not smooth out the B-C resonances completely. Another important feature of the AC treatment discussed here is the appearance of long right-side tails of the B-C resonances. The left-side tails ($u_0 < u_c$) become even more steeper, because under AC conditions electrons spend only a little time near the B-C resonance.

The most interesting experimental results on nonlinear WS transport were obtained employing liquid ^4He [5, 7]. In this case even for $T \sim 0.5 \text{ K}$ the ripplon damping parameter given by Eq. (7) is extremely small. First, we assume that ω is low enough to make Eq. (14) applicable. The comparison of results obtained for the two kinds of averaging of the electric field (E_ω and $\langle |E| \rangle$) is given in Fig. 6, assuming that the velocity is along the NN-direction and $\nu_e = 0$. Here the sharp peaks of the DC model (dotted line) are strongly smoothed by the time averaging of the AC model (E_ω is shown by the solid line, and $\langle |E| \rangle$ - by the dashed line). Additionally, the

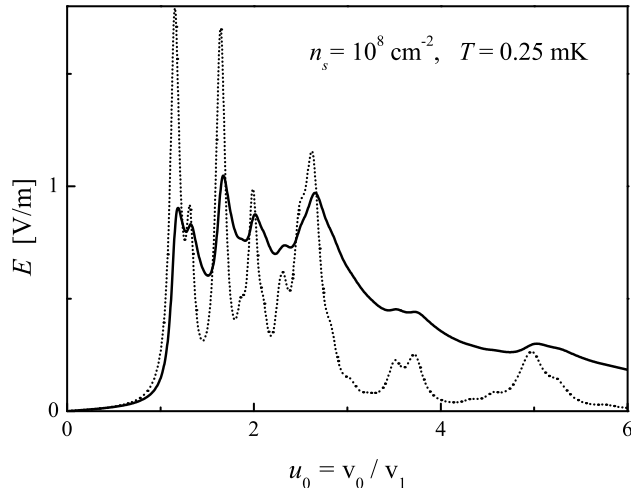


FIG. 5: Field velocity relationship for the DC case (dashed line), and the first Fourier coefficient of the driving field E_ω vs the drift velocity amplitude for the AC case (solid line). Drift velocity is oriented along the NN-direction. Calculations were performed for superfluid ^3He , $n_s = 10^8 \text{ cm}^{-2}$, $T = 0.25 \text{ mK}$.

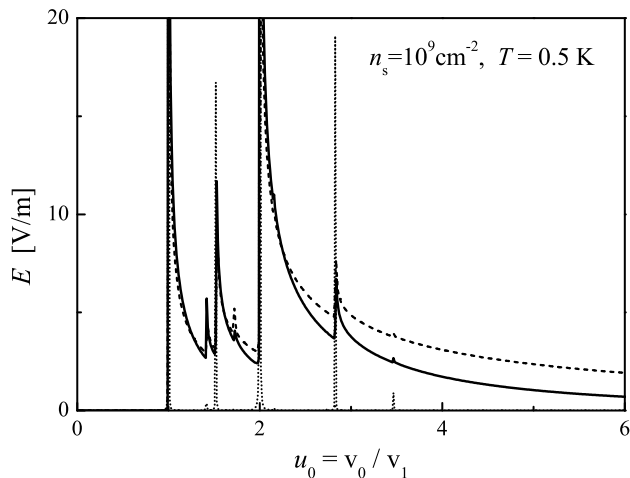


FIG. 6: Field velocity relationship for two kinds of averaging of the alternative driving field: E_ω (solid line) and $\pi(|E|)/2$ (dashed line). Drift velocity is oriented along the SN-direction. Calculations were performed for superfluid ^4He , $n_s = 10^9 \text{ cm}^{-2}$, and $T = 0.5 \text{ K}$ with the ripplon damping parameter defined by Eq. (7).

maximum values of the B-C peaks are greatly reduced as compared to the results calculated for the DC case (dotted line).

The influence of a finite electron collision frequency ν_e due to scattering with thermal ripples and walls is

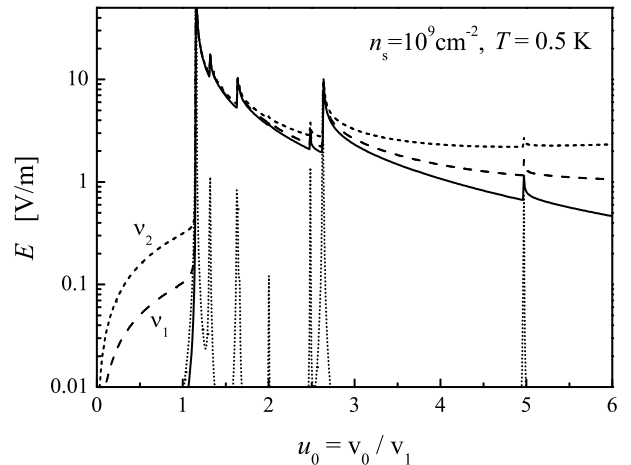


FIG. 7: The main Fourier coefficient of the driving field E_ω vs the drift velocity amplitude for different values of the electron collision frequency ν_e : 0 (solid line), $2.4 \cdot 10^9 \text{ s}^{-1}$ (dashed line), and $7.5 \cdot 10^9 \text{ s}^{-1}$ (short dashed line). Drift velocity is oriented along the NN-direction. The DC case results are shown by the dotted line. Calculations were performed for superfluid ^4He , $n_s = 10^9 \text{ cm}^{-2}$, $T = 0.5 \text{ K}$.

analyzed for the SN-direction and shown in Fig. 7. A reasonable estimate for the electron collision frequency $\nu_e \simeq \nu_1 = 2.4 \cdot 10^9 \text{ s}^{-1}$ (for chosen n_s , E_\perp and T) is found considering electron scattering with thermal ripples in the usual way [2] and taking into account that at low temperatures the average kinetic energy of an electron in the WS state differs substantially from T . For experiments with WS in the channel geometry, ν_e can be even higher because of the WS friction at the channel walls. In order to illustrate this effect in Fig. 7 we considered also a larger value $\nu_e \simeq \nu_2 = 7.5 \cdot 10^9 \text{ s}^{-1}$. According to this figure, the electron collision frequency ν_e affects the both tails of the field velocity characteristic. At the left side ν_e and time averaging of Eq. (13) act in the opposite ways. The left-side tail ($u_0 < u_c$) becomes less steep for a finite ν_e . At the right side ν_e acts in the same way as the time averaging, increasing the right-side tail and making $E_\omega(u_0)$ more flatter in the region $u_0 > u_c$. In general, due to the both these effects the field-velocity characteristic of the WS acquires a distinctive "nose" shape.

The numerical calculations presented in Figs. 6 and 7 were done assuming $\omega \ll \gamma_{g_1}$. In experiments on WS transport over superfluid ^4He this condition was not realized. The influence of the condition $\omega > \gamma_{g_1}$ on the field-velocity characteristics can be understood using the general expressions for $E_\omega(v_0)$ and $Q(w, \beta, \omega')$ given in Eqs. (21) and (22). The main features of B-C scattering under AC conditions can be revealed from the dimensionless function $Q(w, \beta, \omega')$ which describes the shape of a

single B-C resonance [see Eq. (14)]. Consider the main B-C resonance when we can set $w = u_0$, $\beta = 2\gamma_1/\omega_1$ and $\omega' = \omega/\omega_1$, and for simplicity assume $\beta = 0.1$. In the limiting case $\omega' \ll \beta$, the function $Q(u_0, \beta, 0)$ coincides with $Q(u_0, \beta)$ obtained in Eq. (17). For example, it is practically impossible to distinguish $Q(u_0, \beta, 0.001)$ shown in Fig. 8 by the solid line from $Q(u_0, \beta)$ given by Eq. (17). As a function of the dimensionless velocity, $Q(u_0, \beta, 0.001)$ has a typical saw-tooth shape discussed above.

Remarkable shape transformations of $Q(u_0, \beta, \omega')$ as a function of u_0 occur when ω' approaches and exceeds the value of the parameter β which is proportional to ripplon damping. A sharp (from the left-side) saw-tooth peak of a single B-C resonance is developed into distinctive smooth oscillations which [according to Eq. (14)] result in similar oscillations of $E_\omega(u_0)$. The amplitude and the period of oscillations are gradually increase with ω' in the range considered. These oscillations represent a new regime of B-C scattering of the WS which occur under the AC condition, when the current frequency becomes comparable or larger than the ripplon damping.

The period of new conductivity oscillations depends on the relation between the frequency of the current ω and the frequency of ripples excited ω_g . According to Fig. 8, it increases with the ratio ω/ω_g . The ripplon damping just increases the amplitude of oscillations. The later is illustrated in Fig. 9 where $Q(u_0, \beta, \omega')$ is plotted vs u_0 for a fixed value of the ratio $\omega/\omega_1 = 0.05$ and different values of the damping parameter.

There are other important points which follow from Figs. 8 and 9. For low damping the first maximum of the field-velocity characteristic can be substantially larger than the B-C peak value found in the limiting case $\omega \ll \gamma_1$. Secondly, due to the finite frequency ω , even for a very small ripplon damping the left-side tail is not steep as it was for $\omega \ll \gamma_1$. Additionally, the maximum position is substantially shifted to higher drift velocities.

The physics of side-oscillations in the field-velocity relationship can be explained as follows. If $u_0 > u_c$, then even during a period of current oscillations the WS passes through the B-C scattering point four times. The phase difference between surface waves of the same $\mathbf{q} = \mathbf{g}$ excited at different times increases with the velocity amplitude. Thus, depending on the velocity amplitude u_0 the excited waves can interfere constructively or destructively, which is the reason for the side-oscillations. The higher frequency of the current, the larger amplitude is necessary to produce the same phase-difference.

Most of experiments on the nonlinear WS transport are performed using a Corbino geometry of which the alternating current is spatially nonuniform, and only a limited area of the WS can satisfy the B-C scattering conditions. This area changes with time because of the AC conditions. This experimental situation is very difficult to analyze. One may conclude that spatial variations

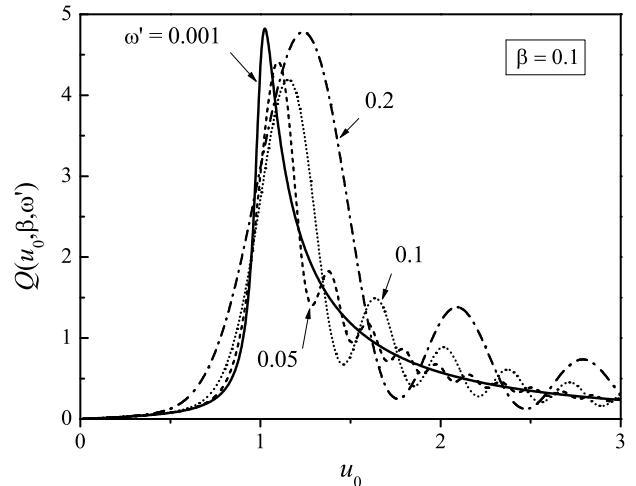


FIG. 8: Shape transformations of the function $Q(u_0, \beta, \omega')$ which describes a single B-C resonance under AC conditions. Calculations are performed for current frequencies: $\omega' = 0.001$ (solid line), 0.05 (dashed line), 0.1 (dotted line), 0.2 (dash-dotted line), 0.3 (dash-dot-dotted line).

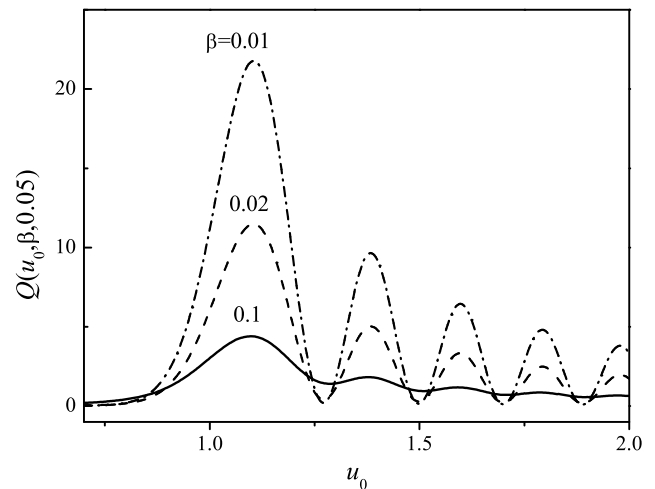


FIG. 9: Shape transformations of the function $Q(u_0, \beta, \omega')$ which describes a single B-C resonance under AC conditions for a fixed frequency ($\omega' = 0.05$) and different ripplon-damping coefficients: $\beta = 0.1$ (solid line), 0.02 (dashed line), and 0.01 (dash-dotted line).

of the current would additionally smooth out the B-C resonances. It should be noted that the field-velocity characteristics of the WS with a "nose" shape without the B-C peaks where observed in the experiment on WS transport in a channel geometry [8]. It is interesting that conductance oscillations similar to the B-C oscillations shown in Fig. 8 were also reported in this experiment.

Therefore, our theoretical results give an alternative explanation for oscillations in electronic response observed for SEs on superfluid helium ^4He .

CONCLUSIONS

In summary, we have analyzed the nonlinear WS transport over superfluid ^3He and ^4He under AC conditions. The theory developed for a spatially uniform alternating current indicates that the field-velocity relationship obtained previously in the classical DC model of B-C scattering is not applicable for time averaged quantities such as the first Fourier coefficient. The detailed analysis is given for two important limiting cases of low and high frequency of the electron current. For frequencies which are much lower than the ripplon damping coefficient, calculations based on the new theory lead to asymmetric B-C peaks of a saw-tooth shape which are strongly broadened at the right side. The broadening of the right-side tails do not depend on small ripplon damping. The left-side tails of the B-C resonances become even steeper which preserves the main B-C anomaly in the field-velocity characteristic.

For current frequencies which are comparable with the ripplon damping or even higher, the new nonlinear regime of B-C scattering of the WS is reported. In this regime each B-C peak is transformed into an oscillatory field-velocity relationship due to interference of ripples multiply excited at different times. The evolution of surface displacements of the dimple sublattice with increasing the current amplitude calculated in this work, as well as the new field-velocity relationships obtained for alternating current, help to understand the nonlinear conductivity of the WS on superfluid helium observed in different experiments.

ACKNOWLEDGMENTS

The work is partly supported by the Grant-in-Aids for Scientific Research from Monka-sho.

-
- [1] In *Electrons on Helium and Other Cryogenic Substrates*, ed. by E.Y. Andrei, Kluwer Academic Pub., Dordrecht (1997).
 - [2] Yu.P. Monarkha and K. Kono, *Two-Dimensional Coulomb Liquids and Solids*, Springer-Verlag, Berlin Heidelberg (2004).
 - [3] C.C. Grimes and G. Adams, *Phys. Rev. Lett.* **42** (1979) 795.
 - [4] D.S. Fisher, B.I. Halperin, and P.M. Platzman, *Phys. Rev. Lett.* **42** (1979) 798.
 - [5] A. Kristensen, K. Djerfi, P. Fozooni, M.J. Lea, P.J. Richardson, A. Santrich-Badal, A. Blackburn, and R.W. van der Heijden, *Phys. Rev. Lett.* **77** (1996) 1350.
 - [6] M.I. Dykman and Yu.G. Rubo, *Phys. Rev. Lett.* **78** (1997) 4813.
 - [7] K. Shirahama and K. Kono, *Phys. Rev. Lett.* **74** (1995) 781.
 - [8] P. Glasson, V. Dotsenko, P. Fozooni, M.J. Lea, W. Bailey, and G. Papageorgiou, *Phys. Rev. Lett.* **87**, (2001) 176802.
 - [9] V.E. Syvokon, K.A. Nasedkin, and A.S. Neoneta, *Fiz. Nizkh. Temp.* **34** (2008) 761.
 - [10] H. Ikegami, H. Akimoto, and K. Kono, accepted for publication in *Phys. Rev. Lett.*
 - [11] H. Namaizawa, *Solid State Commun.* **34** (1980) 607.
 - [12] Yu.P. Monarkha and V.B. Shikin, *Sov. J. Low Temp. Phys.* **9** (1983) 471 [*Fiz. Nizkh. Temp.* **9** (1983) 913].
 - [13] W.F. Vinen, *J. Phys.: Condens. Matter* **11** (1999) 9709.
 - [14] K. Shirahama, Yu.P. Monarkha, and K. Kono, *Phys. Rev. Lett.* **93** (2004) 176805.
 - [15] Yu.P. Monarkha and K. Kono, *J. Phys. Soc. Jpn.* **74** (2005) 960.
 - [16] P. Roche, M. Roger, and F.I.B. Williams, *Phys. Rev. B* **53** (1996) 2225.